Journal of Materials Chemistry C

Accepted Manuscript

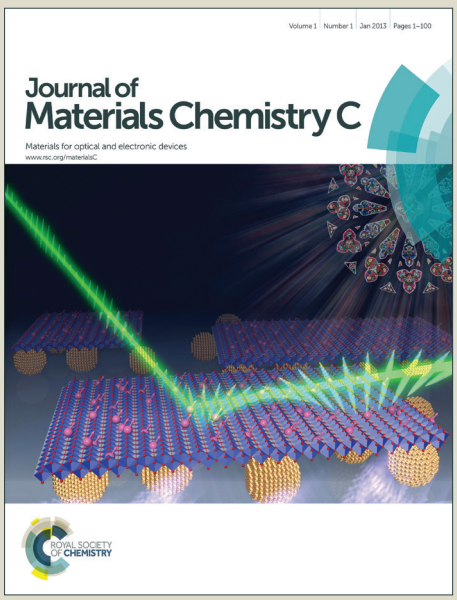

ROYAL SOCIETY OF CHEMISTRY

www.rsc.org/materialsC

Journal of Materials Chemistry C

RSCPublishing

ARTICLE

A Two-Faced "Janus-like" Unimolecular Rectifier Exhibits Rectification Reversal

Cite this: DOI: 10.1039/xoxxoooooox

M. S. Johnson[a], R. Kota[b], D. L. Mattern[c], C. M. Hill[d], M. Vasiliu[d], D. A. Dixon[d], and R.M. Metzger*[a,d]

Received ooth August 2014,
Accepted ooth *** 2014

DOI: 10.1039/xoxxoooooox

www.rsc.org/

A molecule containing an electron donor (pyrene, Py), an insulating tetramethylene bridge, an electron acceptor (perylene bisimide, PBI) and a bis-decyl swallowtail with two terminal thioesters was studied for its electrical rectification as a Langmuir-Blodgett (LB) monolayer between two Au electrodes at room temperature (over a 8-month period, the thioester terminations chemisorbed partially (about 15%) onto the bottom Au electrode). At lower bias (< ±1.5 Volts), the direct current was greater at positive than negative bias; at higher bias (±2.0 and ±2.5 Volts), the conduction was larger at negative bias: this "Janus" switching was repeatable when the bias ranges were changed. At constant bias range, repeated scans showed a gradual decrease in conductivity. Ancillary characterization data are reported.

1. Introduction

Molecular Electronics started with a seminal paper by Aviram and Ratner (AR)[1], who proposed a one-molecule D-B-A rectifier of electrical current (D = strong electron donor, B = covalently bonded bridge, A = strong electron acceptor; AR used a saturated "σ" bridge). Much progress has been made in realizing unimolecular rectification and in measuring the electrical conductivity of single molecules and monolayers[2]. The properties of eleven D-B-A rectifiers of rather diverse structure have been measured at the University of Alabama[2]; other rectifiers have been measured elsewhere[2]. The present goal is to find new rectifiers that pack well enough as either physisorbed Langmuir-Blodgett (LB) monolayers, or as chemisorbed self-assembled monolayers, so that the monolayer is sufficiently rigid, or each molecule is sufficiently bonded to one electrode, that the molecules should not migrate or randomize the molecular ordering under bias, and thus preserve the electronic asymmetry.

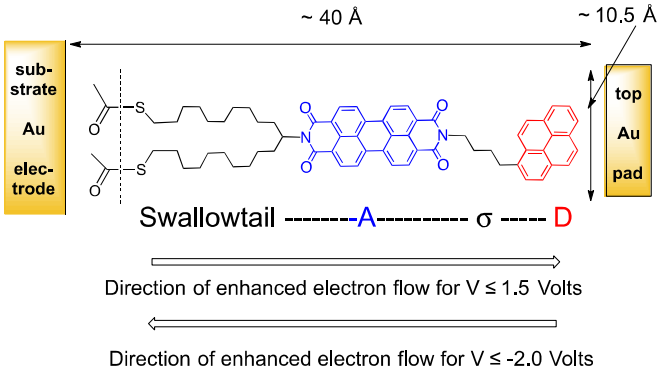

Fig. 1. Schematic structure of **1**, its electronic D-σ-A nature, and its presumed geometry when a LB monolayer of **1** is sandwiched between Au electrodes. From the length estimate shown and a van der Walls thickness of 4.5 Å, the estimated edge-on molecular cross-sectional area is 10.5 Å × 4.5 Å = 47 Å^2/molecule. The vertical dashed line indicates where the homolytic bond scission occurs over time in contact with the substrate Au electrode. The directions of enhanced forward electron flow for |V| ≤ 1.5 Volts and its "Janus-like" enhanced reverse flow for |*V* | ≥ 2 Volts are shown as open arrows.

Rectification by monolayers of eleven different chemical systems has been reviewed recently[2]; in one instance a change in direction of the rectification has already been seen[3]. Other groups have reported rectification for a single molecule chemisorbed in a scanning tunneling break junction[4], and in a ferrocene-alkane-thiolate monolayer on Au studied using a GaIn eutectic top electrode[5]. While molecular wires have symmetric *IV* characteristics (i.e. symmetric in the first and third quadrants), rectifiers should have asymmetric *IV* characteristics (*I* is the electrical current; *V* is the applied DC voltage). However, even molecular wires can behave strangely[6].

In the new donor-bridge-acceptor molecule (*N*-(1,21-heneicos-11-yl)-N′-(4-1-pyrenylbutyl)-perylene-3,4,9,10-bis(dicarboximide) **1**, **Fig. 1**), we start, as in previous work[7], from the one-electron acceptor perylenebisimide (PBI), but now have a 4-carbon saturated bridge, the moderate one-electron donor pyrene (Py), and a pendant group to aid both immediate LB film formation and slower chemisorption to a gold electrode. The synthesis of **1** has been reported elsewhere[8]. "Cold Au" has been used as the top electrode[9], and is used here. Recently, instead of this top pure Au electrode, drops of Hg[10] or a Ga-In eutectic (EGaIn) have been used[11-13] to study molecular conductivity; the internal resistance of most molecules is at least 2 orders of magnitude higher than that of the surface oxide on either Hg or EGaIn[11-13].

For molecular wires several symmetrical *IV* equations have been used to characterize *I* (or the current density *J*) as a function of *V*: they are based on the Wentzel-Kramers-Brillouin-Jeffreys (WKBJ) or "quasi-classical"[14] solutions to the Schrödinger equation: the Fowler-Nordheim (FN) equation[15], the Simmons equation[16-18], the Stratton equation[19], and the Newns-Anderson (NA) equation[20-24]. For molecular wires the Simmons equation worked well[25], but at higher potentials FN behaviour is seen. For

rectifiers, the NA equation was used once[23]. These equations are discussed below.

2. Experimental and Theoretical Methods

The experiments on **1** were divided between (i) molecular characterization (theory and electrochemistry), (ii) monolayer formation at air-water interface, (iii) the LB monolayer orientation, thickness, transfer onto Au electrodes and chemisorption, and (iv) DC electrical properties (*IV* curves) of "Au | LB monolayer | Au" sandwiches. Finally, (v) these *IV* curves were probed using existing theoretical models. A flowchart of theory and experiment is given in Electronic Supplementary Information **(ESI) Fig. A1.**

Following our previous approach[7], energy and geometry minimizations were performed on **1** by using the semi-empirical molecular orbital (SEMO) theory, with the PM6 parameters[26] followed by time-dependent density functional theory (TD-DFT[27,28]) calculations on the first 20 excited states, at the B3LYP[29,30] level with the DZVP2 basis set[31] in both the gas phase and also in $CHCl_3$ (self-consistent reaction field (SCRF[32]) with COSMO parameters[33,34]), to compare the 3 main closely spaced optical transitions. $CHCl_3$ was chosen to model a moderately polar organic solvent regime and is the solvent used (but deuterated) to generate the LB film. All calculations were done with Gaussian09[35].

Electrochemical characterization of **1** was carried out via cyclic voltammetry on films drop-coated[36] onto a Pt electrode in a 0.1 M $LiClO_4$ in CH_3CN electrolyte. Given the very small amount of sample available, a solution phase cyclic voltammogram could not be obtained. Pt and Ag wires were employed as counter and quasi-reference electrodes, respectively. Potentials are reported vs. the value of the ferrocene (Fc^+/Fc) reduction potential obtained using the same electrodes/electrolyte system.

Bottom Au electrodes were prepared by vapor deposition in an Edwards 306A evaporator onto commercial Si substrates with 0.1 - 0.2 nm RMS roughness (University Wafers). The deposition thickness was monitored with a built-in quartz crystal microbalance (QCM). The QCM was at the same distance from the source (about 18 cm) in the evaporator as the Si wafer. First, a 10 nm Cr (VWR) adhesion layer was deposited onto the Si at a constant pressure of 4.5×10^{-6} Torr. Next, 100 nm of Au (VWR) were deposited atop the Cr at 4.5×10^{-5} Torr, at a rate of 0.01 nm sec^{-1}, to maximize the smoothness of the evaporated metal; the last 10 nm of Au were deposited at 0.01 nm min^{-1}.

While the evaporator was cooling down at the end of this first Au evaporation, a NIMA (now KSV, Coventry, England) 622D film balance (Langmuir trough) was prepared, using Barnstead resistivity 18.3 MΩ cm water. The subphase was kept at a temperature of 10°C. The evaporation chamber, still warm to the touch, was opened, and the "Si/Cr/bottom Au" substrate was placed within less than 5 min under conductivity water at the bottom of the Langmuir trough: this ensured a hydrophilic Au surface, checked by measuring the contact angle with water.

The two movable computer-controlled Teflon barriers were opened (maximum area = 1300 cm^2) then closed (minimum area = 180 cm^2), and the surface of the subphase was aspirated to remove contamination. Finally the barriers were re-opened and a solution of **1** in $CDCl_3$ was added drop-wise. A wait time of 20 min allowed for equilibration of the water evaporation rate and of the Wilhelmy plate surface tension sensor. After evaporation of the $CDCl_3$ solvent, an insoluble Pockels-Langmuir (PL) monolayer[2] of **1** formed at the air-water interface; its formation was monitored using the NIMA software on a PC microcomputer. As a control, a freshly poured subphase of water showed a surface tension decrease of -1.5 to -2 mN/m over a 30-minute period.

A closely packed LB monolayer of **1** was transferred to a "Si/Cr/bottom Au" substrate on the first upstroke. After the LB film transfer, the "Si | Cr | Au | LB monolayer of **1** open-faced sandwich" was dried overnight in a vacuum desiccator to remove adventitious water. The same was done for the monolayers transferred onto glass and Si.

XPS spectra were measured in a Kratos Axis 165 photoelectron spectrometer. All high-resolution spectra were taken at a pass energy of 40 eV, with wait times of 1 second per data point for O and C. S and N high-resolution spectra were taken with a wait time of 5 seconds, in an attempt to maximize and resolve the photoelectron signal. The experiment was taken at the magic angle (55°), making the measurement more surface-sensitive. The spectra were visually fitted using a Shirley background correction to a 70% Gaussian - 30% Lorentzian peak shape equation:

$$F(E) = h\,(1-M)/[1 + ((E-E_0)/(\beta+\alpha(E-E_0)))^2] + h \times M \times [\exp(-\ln_e 2\,((E-E_0)/(\beta+\alpha(E-E_0)))^2] \quad (1)$$

where E is the binding energy (eV), h is the experimental peak height at energy E_0, β is the peak width, α is a peak asymmetry (here $\alpha = 0$), and $M = 0.70$[37]. All curves were corrected using the adventitious C(1s) signal at 284.8 eV. The areas under the curve for each element were corrected by a corresponding elemental relative sensitivity to measure the atomic concentration of the elements.

UV-visible absorption spectra were measured in a Varian Cary 50 spectrometer in transmission mode for two monolayers of **1** on a glass slide (one monolayer per side); two photographic polarizing filters, placed parallel to the plane of the glass slide, were used to determine the orientation of the optical transition moment(s)[3]: the analyzer filter could be rotated by an angle ω relative to the polarizer filter (ω=0° for parallel, ω=90° for perpendicular orientation = "crossed" polarizers).

The monolayer thickness was measured using a J. A. Woolam VB-250 VASE multi-angle ellipsometer using a Cauchy fit to the data.

Atomic force microscopy (AFM) was used for additional thickness measurements, as well as for the overall structure of the monolayer on the silicon substrate. A Bruker Multi-Mode 8 AFM was used with a Digital Instruments Nanoscope V controller. SCM-TIC tips with factory-estimated force constants of 0.2 N/m were used in contact mode. Thermal tune was used for each tip to get an accurate force constant. Images were taken in both height mode and deflection mode. The X, Y, and Z sensitivities were calibrated using a 4 μm pitch grid with ~25 nm step sizes (Nanoscience Instruments). The heights attained for the grid are within 5% of the estimated value.

To add the top "pad" Au electrodes to the open-faced sandwich described above, it was returned to the evaporator, topped by a contact mask, and placed over a liquid-nitrogen cooled stage; 400 top Au "pads" (square, 1 mm^2 in area per pad, 10-15 nm thick) were evaporated atop the LB monolayer by the "cold gold" technique[9]: the Au vapor was thermalized by adding Ar gas to the evacuated chamber (2×10^{-4} Torr) for an hour, to ensure that any excess moisture was purged from the system before evaporating the gold. When the chamber was presumed to be free of moisture, liquid nitrogen was added[9]. The Au evaporation continued over 100 min; the pad thickness was measured by a properly oriented QCM.

The deposition rate was 0.1 Å/min. At higher concentrations of Ar gas (7.5×10^{-4} Torr) the Au formed black aggregates on the nearest metal surface, and very light or no pads were formed on the solid substrate, even after evaporating 0.5 g Au. In contrast, tiny brown 1 mm^2 pads (presumably nanoparticles of Au) could be seen above the monolayer surface when the cold gold deposition was successful.

For electrical measurements of the monolayer of **1**, the wafer with its top Au pads was placed in a Faraday cage. Electrical contact to the bottom Au electrode was made using a rigid gold-paste-coated clamp. Electrical contact to each top Au pad electrode was made using a micromanipulator and a Au wire that had a drop of EGaIn[11] (Ga-In eutectic liquid) suspended in a shape that varied from spherical to cone-like; cone-like drops were used to make contact[9]. The suspension of the EGaIn drop ensured that only EGaIn contacted and wetted the top pad and that the Au wire did not pierce the top pad (which would have short-circuited the junction).

Sequential electrical contact to any of the 400 top Au pads investigated by the hanging EGaIn probe was controlled by setting the external voltage at 0.1 mV, then lowering the EGaIn contact to the pad using the micromanipulator, and searching for currents in the nA range (0.01 nA to 10 nA): this is a procedure similar to that used in STM measurements. A Keithley Model 236A Source/Measure Unit, controlled by a Labview® computer program on a PC micro-computer, collected the IV data: the minimum reliable current measurable by the Keithley unit is $I_{min} \approx 1$ pA, i.e. $\ln_e(I_{min}$ / Ampères) ≈ -27.6 . Whenever currents at $V = 0.1$ mV rose above 10 nA, short-circuits would result for a scan range of ±1 V; in contrast, when currents at 0.1 mV were between 0.01 nA to 10 nA, then reliable scans with large bias (up to ±3.0 Volts) could be performed.

The "Au wire | Au paste | bottom Au electrode | LB monolayer of **1** | 'top Au electrode' | EGaIn | gold wire" sandwiches were then studied for their direct current (I) vs. voltage (V) electrical behavior.

The rectification ratio RR is defined by:

$$RR \equiv I(V) / | I(-V) | \quad (2)$$

and depends on which maximum (minimum) voltage V is chosen.

As in previous work[9], to ensure that the results reported here are not due to electrode artifacts, the full procedure described above was checked with a monolayer of arachidic acid. The arachidic acid data always showed the normal non-linear but symmetric IV curve typical for tunneling through a LB monolayer of a saturated hydrocarbon chain.

3. Results

3.1. Molecular characterization (theory and electrochemistry)

Theory. After geometry optimization, the HOMO-LUMO gap was 1.58 eV at the DFT level. Plots of the HOMO-1, HOMO and LUMO amplitudes are shown in **Figs. 2** to **4**. The HOMO-1 and LUMO amplitudes are concentrated on the PBI moiety. The molecule is slightly bent. The HOMO-1 to LUMO transition is the first one with a significant oscillator strength (f = 0.83) and is predicted to be 2.17 eV with λ_{max} = 537 nm. In $CHCl_3$ solvent the transition is predicted to be 2.17 eV (λ_{max} = 570 nm), with f = 1.00. The calculated HOMO energy of **1** (-5.51 eV) differs considerably from the experimental gas-phase vertical ionization potential of Py (I_D = 7.41 eV[38]), as is typically observed in DFT calculations[39]. The LUMO energy of **1** (-3.93 eV) differs from the calculated electron affinity of PBI (A_A = 2.28 eV[40]). Other literature values are: for Py the gas-phase electron affinity is 0.390 eV[41]; for PBI the calculated vertical ionization potential is 7.43 eV[40]. We note that the experimental work function for pure (Hg-free and adsorbate-free) polycrystalline Au is 5.20 eV[42].

Previous calculations on a molecule very similar to **1** gave a HOMO-LUMO gap of near zero at the DFT level, but of 0.65 eV (at the SVWN level of DFT), or 1.60 eV (at the DFT level after correcting the asymptotic form of the correlation potential)[7,43].

The molecular length from the calculated optimized structure shown in **Figs. 2** to **4** is 3.8 nm (as compared with the crude value of 4.0 nm from the planar molecular structure drawn in **Fig. 1**). More energy levels are shown in **ESI Table A**.

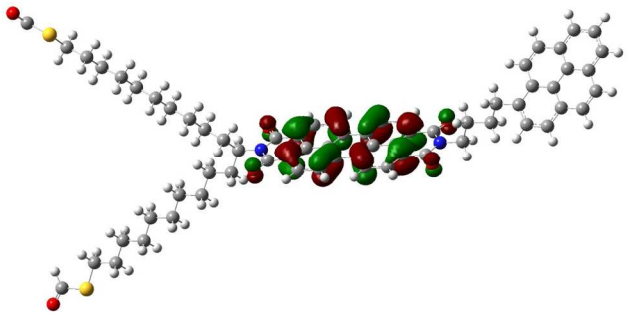

Fig. 2. The DFT HOMO-1 is concentrated on the PBI moiety.

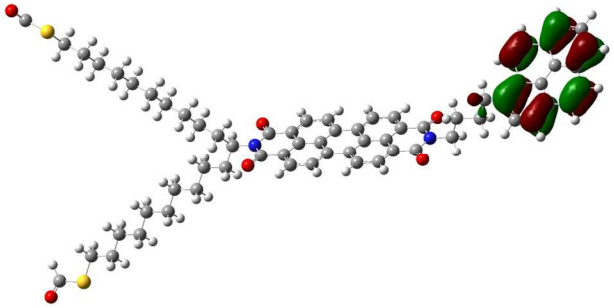

Fig. 3. The DFT HOMO is mostly concentrated on the Py moiety.

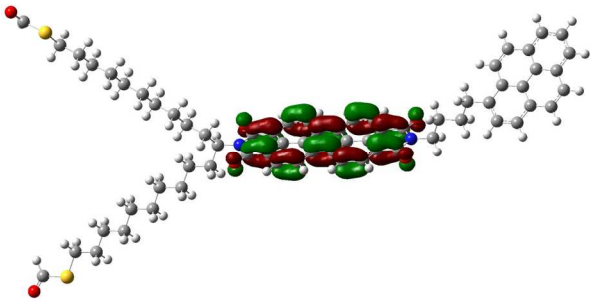

Fig. 4. The DFT LUMO is mostly concentrated on the PBI moiety.

Electrochemistry. The cyclic voltammogram, or microelectrochemical potential spectrum,[36] of a drop-coated film of **1** is shown in **ESI Fig. A2**. The first oxidation and first reduction peaks are at 1.45 V and -0.89 V *vs.* Fc/Fc^+, respectively. These peaks compare well with the known first oxidation of Py at 1.44 V

vs. Fc/Fc^+ in CH_3CN[44,45] solution, but less well with the first reduction of PBI at -0.98 V *vs.* Fc/Fc^+ in CH_3CN[46] solution.

3.2. PL monolayer formation at air-water interface

The surface pressure-area ($\prod$-A) isotherm of **1** for a dilute dropping solution (100 µL of 0.1 mg mL^{-1} **1** in $CDCl_3$, 3.67 × 10^{-4} M) is shown in **Fig. 5**. If more concentrated solutions of **1** were used, then the isotherms showed evidence of pre-association (**ESI Fig B1** and ensuing discussion): this pre-association is well known for H-aggregates of PBI[47] and also for C_{60}[48]. **ESI Fig. B2** shows that at a constant surface pressure ($\prod_t$ = 18 mN/m), the measured cross-sectional molecular area decreased gradually over 25 min from 70 Å^2/molecule (**Fig. 5**) to A_t = 55 Å^2/molecule (**Fig. B2**), at which area the monolayer islands touched each other, and the molecules were packed into a single pink, compact floating monolayer.

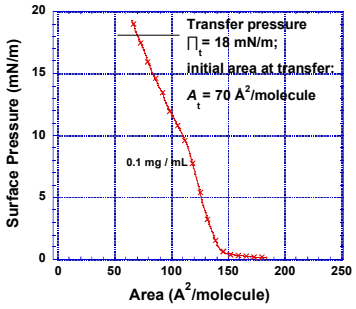

Fig. 5. Pressure-area isotherm (PAI) of **1** at 10°C (spreading solution: 100 µL 0.1 mg/mL **1** in $CDCl_3$). The adopted transfer pressure is 18 mN/m; the initial area at the transfer pressure (before "annealing") is 70 Å^2.

3.3. LB monolayer transfer, thickness, and orientation

LB transfer. After allowing the monolayer to reach equilibrium at this constant pressure (as shown after 25 min in **ESI Fig. B2**), an LB monolayer was transferred onto the "Si/Cr/bottom Au" substrate on the upstroke at $\prod_t$ = 18 mN/m, at 1 mm/min, with a collapse area of roughly 55 Å^2/molecule. No transfer was observed on a first down-stroke. The pink floating islands could be seen to move towards the substrate during the up-stroke transfer. After the transfer, monolayers were visible on the surface of gold substrates; they could also be seen by the naked eye after breathing on silicon substrates. The PBI chromophore gave a pink color to glass substrates covered by monolayers. Given what happens at $\prod_t$ = 18 mN/m (**ESI Fig. B1**), the transfer ratio of **1** could not be measured directly. Qualitatively, the transfer ratio onto Au was similar to that onto Si, as seen by eye after the transfer. The coverage of each substrate was roughly 80% and large uniform areas (cm^2) of monolayer could be seen. The monolayer transferred without entraining water, so each sample emerged from subphase looking dry, without any residual water present.

UV-visible absorption spectra. An LB monolayer of **1** on both sides of a glass slide was pink. The UV-Vis spectrum (**ESI Fig. C**) showed three peaks with λ_{max} = 476, 503, and 540 nm. The UV-Vis spectra of similar molecules in isotropic $CHCl_3$ solution have peaks, due to the PBI moiety, at 461, 491, and 527 nm[7] (**ESI Fig. D1**). The peak at 540 nm may be related to a concentration and temperature-dependent π-π intermolecular association (it is seen in related PBIs between 529 and 541 nm[47]). The caption to **ESI Fig. C** documents the efforts to determine the orientation of the PBI moiety within the LB monolayer by measuring the polarized absorption[3] as a function of macroscopic rotations of the monolayer-bearing glass slide.

X-ray-photoelectron spectroscopy: which end of the monolayer is "up"? Is there chemisorption? The monolayer was probed using XPS to gain insight on the bonding and orientation of the LB monolayer, and compared to a "bulk" (>30 nm thick) LB multilayer sample. To see the N(1s) and S(2p) peaks of **1** in the monolayer, high-resolution spectra were measured with a pass energy of 40 eV and wait times of 5 seconds. The results are given in **Fig. 6** ("bulk" LB multilayer of **1**) and **Fig. 7** (LB monolayer of **1**). That the S atoms in **1** are close to the Au substrate was indicated by comparing the spectra of the "bulk" sample of **1** (**Fig. 6**) with that of the monolayer of **1 (Fig. 7)**. By integration of the XPS peaks in the "bulk" spectrum, the S(2p) and N(1s) concentrations were similar (1.18% for S, 1.37% for N). In the LB monolayer spectrum, the concentrations are 1.17% for S but 2.54 % for N. This strongly suggests that the N atoms are closer to the outer surface (vacuum), while the weaker and broader S peaks are closer to the detection limit (the inelastic mean free path for S is 1 nm). This is also evident by the lack of resolution of the monolayer S(2p) peak vs. the great resolution of the monolayer N(1s) peak. The three peaks from the S(2p) are likely from the thioester alone (164.15 eV), a weak thioester-gold complex (163.75 eV), and the thiolate (161.9 eV). Therefore, the thioester terminations of **1** are close to the Au "bottom" electrode.

The high-resolution spectra of the S(2p) in a "bulk" sample (**Fig. 6(b)**) and in the LB monolayer (**Fig. 7(b)**) showed a small thiolate peak (161.9 eV) in the monolayer sample, which were absent for the bulk sample. Furthermore, an older monolayer of **1** (which probably was not packed as well as this monolayer) showed only thiolate peaks after two months in air. The thiolate peak will appear if the thioester S has reacted with the substrate Au; since no base was added in any of these experiments, a homolytic scission

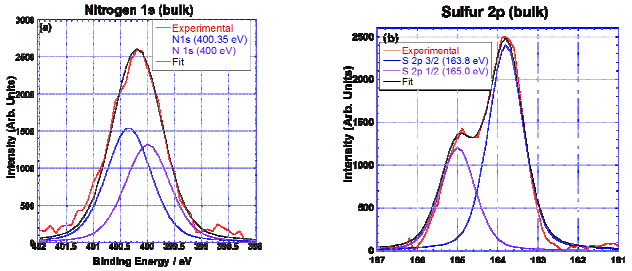

Fig. 6. XPS spectra for "bulk" sample of **1** on Au. **(a)**: N(1s): peaks at 400.35(main) and 400 eV **(b):** S(2p): peaks at 163.80 eV (2p 3/2) and 165.0 eV (2p 3/2).

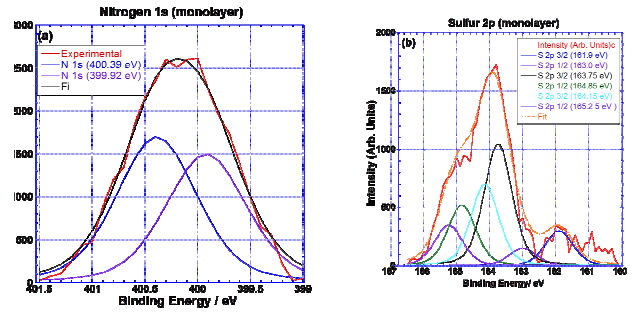

Fig. 7. XPS for monolayer of **1** on Au: **(a)** N(1s): peaks at 399.92 (main) and 400.39 eV; **(b)** S(2p 3/2 & 2p 1/2): peaks at 161.9 & 163.0, 163.75 & 164.85 (main), and 164.15 & 165.25 eV.

of the S-C bond should be a very slow process, and the S(2p 3/2) peak at 161.9 eV should grow slowly over time, as observed.

The partial polarity of the S-Au bond probably contributes ca. 2 D to the dipole moment of the molecules covalently attached to the Au electrode[49].

Ellipsometry: how thick is the LB monolayer? The thickness for an LB film of **1** transferred at 18 mN/m onto Si was measured by spectroscopic ellipsometry as 3.7 ± 0.1 nm, i.e. not far from the estimated molecular length of 4.0 nm (**Fig. 1**) and the calculated molecular length of 3.8 nm (**Figs. 2** to **4**).

AFM: how thick is the LB monolayer? The AFM image (**ESI Fig. D2**) showed a well-ordered monolayer, but with whitish spots (multilayer) formed at grain boundaries. Using two random defect spots, the monolayer thickness was estimated as 3.3 nm.

3.4. DC electrical properties

An important issue was whether some of the rectification discussed below could be ascribed to the asymmetric junction created when Ga_2O_3 forms at the surface of a drop of GaIn eutectic in air[11] (but disappears upon complete alloy formation with Au) (**ESI Figs. E, F,** and **G**). To test this, simple "wire | Au paste | 'bottom Au' electrode | EGaIn | Au wire" sandwiches[11] were investigated as controls (no molecule **1**). The EGaIn-wetted wire was used directly as the top contact to the bottom Au electrode (no top Au pad and no organic monolayer): this should yield the IV characteristics of a "GaIn/Ga_2O_3/Au" junction in the absence of an organic monolayer. Two sets of reproducible IV curves did show rectification: (i) The first set started with an ohmic (linear) IV curve that reached a maximum at 0.3 V, then became more resistive; successive scans up to ±1 Volt showed a maximum current of 100 nA at 1 Volt that was both non-linear and asymmetric, with RR as high as 10. All these sandwiches failed by short circuits if the scan range was extended beyond ±1 V. We believe these observations evidence the formation of additional Ga_2O_3 through bias-induced redox reactions at the surface; Ga_2O_3 is an n-type semiconductor[11] that can act as a Schottky barrier. (ii) The second set resembled the behavior of junctions of molecular insulators with Au: it was non-linear (RR=4 in first cycle), but became symmetric after 2 cycles. Neither set of these IV measurements of EGaIn resembled the IV behavior of monolayers of **1** shown below.

Of the 400 top Au pads available, 54 were studied in detail over one year's time. The geometry of the electrodes, relative to the molecules in the LB monolayer, and consistent with the XPS data given above, is sketched in **Fig. 1**. The direction of initial enhanced electron flow (forward rectification) and of final enhanced electron flow at negative bias (reverse rectification) is also indicated in **Fig. 1**, on the basis of the *IV* curves discussed below.

Initially some pads were studied too rapidly in the voltage range ±1 V, and electrical short-circuits developed. As mentioned above, increasing the scan range slowly by 0.2 V increments, and making measurements in 0.01 V steps, "annealed" or "tempered" the junction; thereafter, up to 70 repeated and reliable measurements were possible on the same pad. This annealing may be due to some Joule heating: in a conducting-tip break-junction AFM study of 1,8-octanedithiol, a temperature increase of 30 K at a bias of 1 V was estimated[50].

ESI Table B1 summarizes results for the most interesting and well-studied 6 pads, while the data for all pads are listed in **ESI Table B2**. Pad 42 was measured 3 days after sandwich assembly; pads 45, 46, and 48 were measured 3 months after assembly; pads 52, 53, and 54 were measured 8 months after assembly. The estimates for "onset" and for "rectification" are visual. Assigning an onset voltage for rectification (V_{rect}) is complicated by the vibrational broadening of the donor and affinity levels, i.e. by where exactly, in **Figs. 8** to **12**, one should pinpoint the onset of an enhanced current (V_{onset}).

Several phenomena were observed:

(i) **Forward rectification ratio**. Asymmetric *IV* curves gave "forward" rectification in the direction shown in **Fig. 1** when $|V_{max}| \leq 1.5$ V, but the conductance and rectification ratio *RR* both decreased upon repeated scanning (**Fig. 8**). Pad 42 showed a reasonably consistent $RR \approx 14$ when it was cycled multiple times up to $|V_{max}| = 1.0$ Volt.

(ii) **Reversal of rectification**. The direction of rectification was reversed ("Janus" effect) when $|V_{max}|$ increased to 2 V (**Fig. 9**) or 2.5 V (**Figs. 10** and **11**). Such high voltage ranges (±2.0 to ±2.5 V) were not accessible in many earlier studies of different D-B-A rectifiers: short circuits would develop. However high-voltage measurements were successful in an STM experiment,[51] and, for a very rigid monolayer, rectification reversal was observed[3].

(iii) **Evolution of chemisorption over time**. Measurements were possible even 8 months after the pads had been fabricated (Pads 52 and 54), and even though by that time the gradual chemisorption would have added an extra interface dipole of probably 2 D at the "Au | molecule" interface[49].

(iv) **Repeatability of rectification reversal**. For pads 52 and 54, one could go back and forth repeatedly between forward rectification (at low V_{max}) and reverse rectification (at high V_{max}) (**Table B2**). Thus one can exclude (a) molecular degradation and (b)

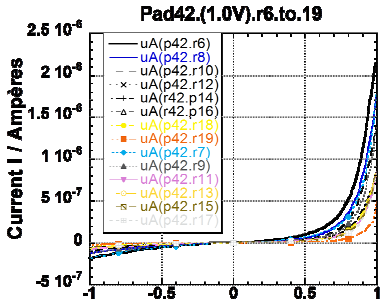

Fig. 8. *IV* curves for a sandwich "Si | Cr | Au | LB monolayer of **1** | Au" (pad 42 runs 6 to 19) in the range $|V_{max}| = 1.0$ Volt. Graphical estimates: $V_{onset1} = 0.4$ Volts; $V_{rect1} = 0.7$ Volts.

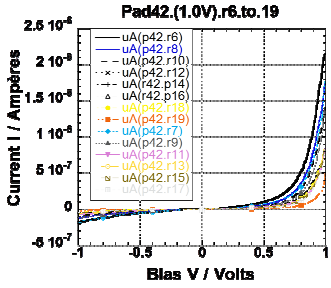

Fig. 9. Repeated full cycles (negative to positive voltage and back) of a sandwich "Si | Cr | Au | LB monolayer of **1** | Au" (pad 42 runs 43 to 46) in successive runs with increasing $|V_{max}|$ to 2.0 Volts. After cycling at this higher voltage, a larger current was seen at negative bias than at positive bias. The reverse rectification ratio (*RRR*) at 2.0 V was 3.24 (pad 42, run 45). Graphical estimates: $V_{onset2} = -1.5$ Volts; $V_{rect2} = -1.8$ Volts.

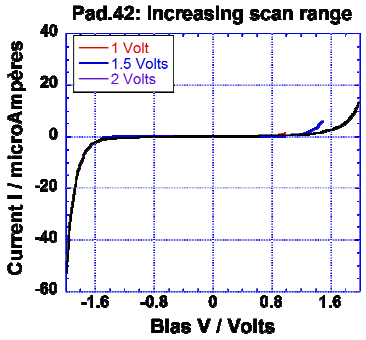

Fig. 10. Repeated cycles of a sandwich "Si | Cr | Au | LB monolayer of **1** | Au" (pad 45) in successive runs with increasing $|V_{max}|$ to 2.5 Volt. Graphical estimates: V_{onset2} = -1.8 Volts, V_{rect2}= -2.2 Volts.

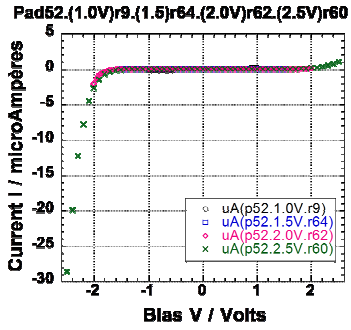

Fig. 11. *IV* curves for a sandwich "Si | Cr | Au | LB monolayer of **1** | Au" (8-month-old "pad 52") in successive runs with $|V_{max}|$ = 2.5 Volts. Graphical estimates: V_{onset2} = -1.6 Volts, V_{rect2}= -2.2 Volts.

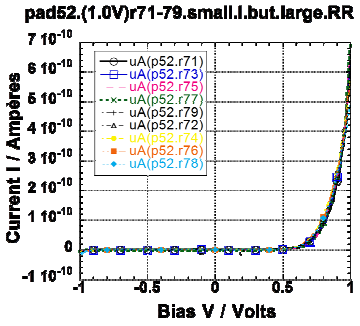

Fig. 12. Small currents and dramatically large rectification ratios (average *RR*=144 for upwards scan, *RR*=93.4 for reverse scan) (8-month–old pad 52, runs 71-79, $|V_{max}|$ = 1.0 Volt). Graphical estimates: V_{onset1} = 0.65 Volts; V_{rect1}= 0.85 Volts.

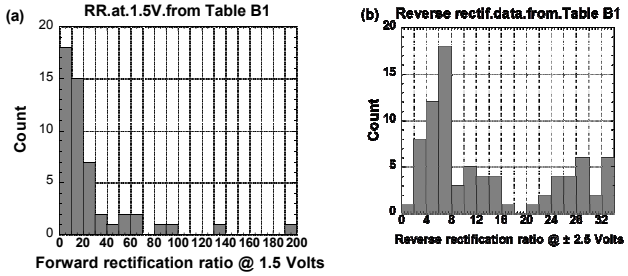

Fig. 13. Histograms of **(a)** *RR* at 1.5 Volts from all data (**ESI Table B1**); (b) *RRR* from all data at 2.5 Volts (**ESI Table B1**).

molecular reorientation, which is impeded by the gradual chemisorption.

(v) **Much higher rectification ratios seen**. For pad 52, with larger resistances and much smaller currents, RR increased dramatically (**Fig. 12**). Such high RR's were not seen for Pad 54.

(vi) **Gradual decrease of monolayer conductivity**. Repeated measurements on the same pad showed a gradual decrease in the currents at $V>0$ and a different decrease in the currents at $V<0$ (**Figs. ET**, **EU**). Such decreases were surprisingly absent for the 20 runs at $|V_{max}|$ = 2.5 V for pad 52 (**Fig. EV**). *RR* is larger for ascending voltages than for descending voltages.

(vii) **Statistics on forward and reverse rectification ratios**. Histograms for forward rectification ratios (*RR*) at 1.5 V and reverse rectification ratios (*RRR*) at 2.5 V, using all data from **ESI Table B2**, are given in **Figs. 13(a)** and **Fig. 13(b)**, respectively. The average <RR> = 26.1 ± 4.98 (standard error) using all 51 data, which become <RR> = 20.5 ± 3.05 if the two high RR=195 and RR=132 data are expunged. The average <RRR> = 14.0 ± 10.4 (standard deviation) or 14.0 ± 1.16 (standard error).

(viii) **Reminder: at high bias the electric fields are large!** A 2.5 V bias across 3.7 nm generates an electric field of 0.67 GV/m. A 1 mm^2 Au top pad should cover 1.8×10^{12} molecules of area 55 $Å^2$/molecule each. A 1 μA current (6.3×10^{12} electrons per second) across that 1 mm^2 pad then corresponds to 3.5 electrons per molecule per second (if the pad is completely metallic).

3.5. Theoretical *IV* curves for rectifiers and transition voltage

Of the *IV* equations based on the WKBJ method we show two of them, and mention two more:

(i) The first, and oldest of these approximate *IV* treatments is the Fowler-Nordheim (FN) equation[15]:

$$J = (e^3 V^2 / 8 \pi h \Phi_B d^2) \exp - (8 \pi d / 3 e h V) (2 m_e)^{1/2} \Phi_B^{3/2} \quad (3)$$

where e is the electronic charge, m_e is the electron mass (or effective mass, if needed), h is Planck's constant, Φ_B is the barrier height (typically the work function of the metal electrode), and d is the barrier width. Valid for relatively large voltages, Eq.(3) was used to explain the "cold thermoionic effect" and works for V high enough that the barrier is triangular rather than trapezoidal.

(ii) The second is the Simmons equation[16-18]:

$$J = (e/4\pi^2\hbar d^2) \{(\Phi_B - eV/2) \exp [-(2d/\hbar) (2m_e)^{1/2} (\Phi_B - eV/2)^{1/2}] + (\Phi_B + eV/2) \exp [-(2d/\hbar) (2m_e)^{1/2} (\Phi_B + eV/2)^{1/2}]\} \quad (4)$$

for small to medium voltages, valid within a trapezoidal barrier region.

(iii) The third is the Stratton equation[19].

(iv) The fourth is the inverse-tangent Newns[20]-Anderson[21] (NA) equation, used for conductivity within molecules[6,22-24].

Plots of experimental log (I/V^2) versus $1/V$ would provide a constant slope if Eq.(3) were valid for all voltages V; in fact these plots most often show a minimum at a "transition voltage" V_{tr}[52-54] presumably because I may follow Eq. (3) at higher V, but Eq. (4) at lower V. For many molecular wires the high-voltage region cannot be explored, because electrical breakdown occurs between 1.5 V and 2.0 Volts[53].

There have been efforts to link V_{tr} to the position of the HOMO level. One assignment is[55]:

$$V_{tr} = 1.15 (\mu - \varepsilon_{HOMO}) \quad (5)$$

where μ is the chemical potential. A different explanation is that V-induced shifts occur in the donor level (ε_{HOMO}) and the affinity (acceptor) level (ε_{LUMO}) until resonance is reached with the relevant (shifted) Fermi level E_F. Then V_{tr} marks a transition between two different regimes of dependence of I upon V[52,54]. Another assignment is[53,56]:

$$V_{tr} = \mu - \varepsilon_{HOMO} \quad (6)$$

Despite an early effort[23], at present for unimolecular rectifiers no single equation seems to apply for all V values; the "plateauing" of I at higher V predicted by the NA equation has only been seen for one rectifier[9]. However, using measured V_{tr} values and either Eq.(5) or Eq.(6) may help to estimate the bias V at which resonance with the HOMO level should provide an increase in current.

The transition voltage V_{tr} observed in molecular wires by other researchers[52,53] is very clearly seen in the approximately vee-shaped plots of $\ln_e(|I|V^{-2})$ versus V^{-1} for $|V_{max}|$ = 1.0 Volt (**Fig. 14**). In contrast, for higher $|V_{max}|$ ranges, the plot becomes L-shaped, with a clear minimum only for a minority of runs (**Fig. 15**).

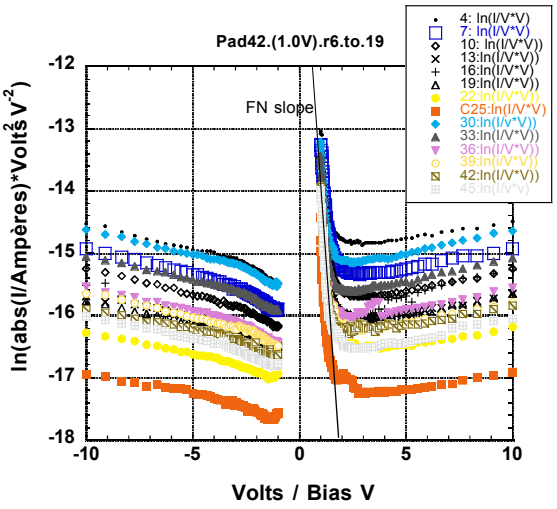

Fig. 14. Plot of $\ln_e(|I|V^{-2})$ versus V^{-1} for pad 42 and $|V_{max}|$ = 1.0 Volt. The transition voltage is V_{tr} = +0.54 Volts for V>0, but V_{tr} = -0.47 Volts for V<0. The Fowler-Nordheim limiting slope is also shown.

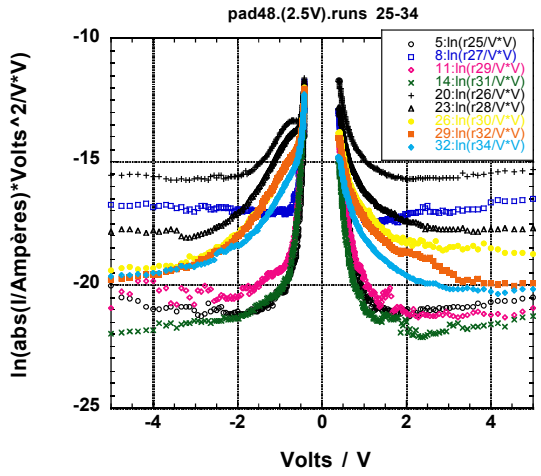

Fig. 15. Plot of $\ln_e(|I|V^{-2})$ versus V^{-1} for pad 48 and $|V_{max}|$ = 2.5 Volts.

ESI shows all the $\ln_e(|I|V^{-2})$ versus V^{-1} plots. In **Fig. 14** there is a clear left-right asymmetry: V_{tr} = +0.54 Volts for V>0, but V_{tr} = -0.47 Volts for V<0. This asymmetry may be due to the acentric placement[6,23] of the significant LCAO coefficients for the relevant molecular orbital.

One is tempted to seek meaningful data from the slope of the "Fowler-Nordheim region" of **Fig. 14**. Using cgs units, for d = 4 nm, V=1 Volt, and Φ_B = 5 eV the exponent of Eq. (4) becomes - (8 π d / 3 e h V) (2 m_e)$^{1/2}$ $\Phi_B^{3/2}$ = -1.02; this number decreases if the customary (smaller) reduced electron mass is used instead of m_e. In contrast, the limiting slope for V>0 from **Fig. 14** is much larger, between -6 and -7, so this temptation must be resisted.

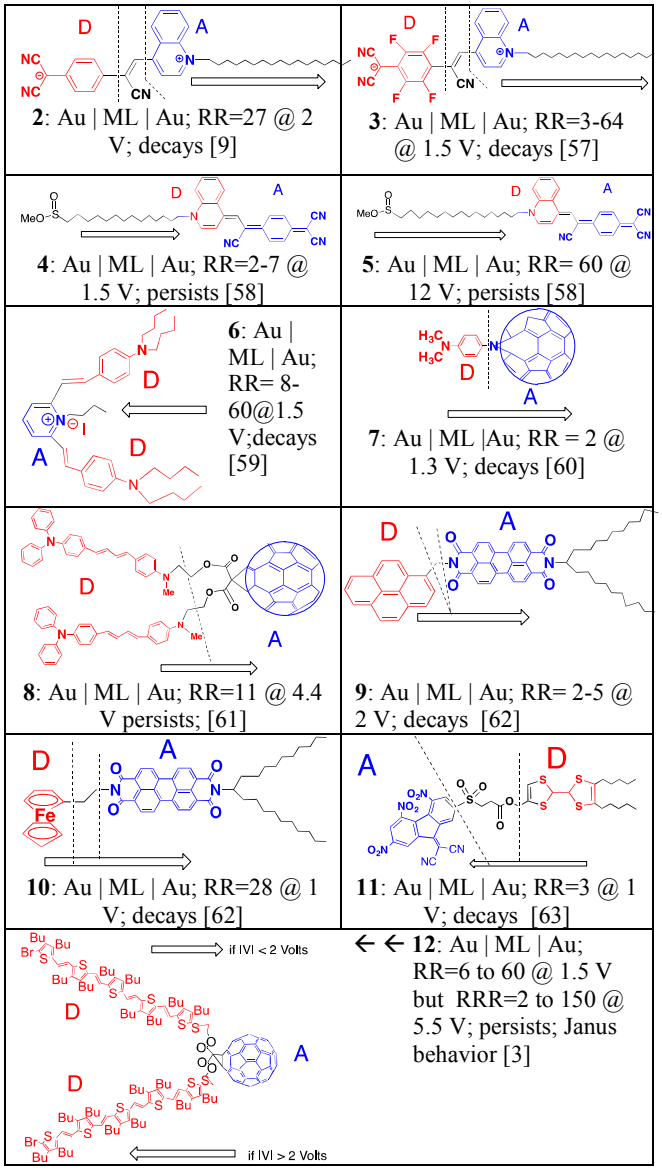

Fig. 16. Rectifiers previously studied in this laboratory[2]. The electron donor moieties (D) are in red; the electron acceptor moieties (A) are in blue. The direction of enhanced current and the rectification ratios *RR* at maximum forward bias are shown with [literature references]. The currents are persistent in **4**, **5** because of chemisorption; they are persistent in **8** and **12** because the monolayer is very rigid and compact. The Janus effect was observed in **12** with reverse rectification ratio *RRR*.

Routine and unremarkable $\ln_e(|I|)$ versus V plots were seen (**ESI Figs I, M, R, V, Z, AD, AH, AL, AR, AV, BD, BH, BL, BP, BT, BX, CB, CF, CJ, CN);** for larger $|V_{max}|$ ranges the $\ln_e(|I|)$ versus V plots show a more complex behaviour. Some plots for pads 52 and 54 show a peculiar bifurcation at low V and low currents, close to the detection limit of the Keithley Source-Measure Unit (**ESI Figs. CS, CW, DA, DG, DH, EI**).

4. Discussion

Molecule **1** tends to aggregate in solution, so dilute dropping solutions were used to form a proper monolayer at the air-water interface. The LB transfer, possible on the upstroke only, confirms that the molecule is amphiphilic (the thioester tail is more hydrophilic than the pyrene head) (this is also confirmed by XPS); over several months, the LB monolayer that was transferred onto Au formed chemisorbed thiolates on Au (increasing the molecular polarity). The LB behavior of **1** is a remarkable contrast to that of a very similar compound (**Fig. 16**, structure **9**)[7].

The LB monolayer film thickness (3.7 ± 0.1 nm by ellipsometry, 3.3 nm by AFM) is smaller than the estimated length of either 4.0 nm (**Fig. 1**) or 3.8 nm (energy-minimized theoretical length: **Figs. 2** to **4**): this suggests that the molecules are tilted 20º to 30º from the normal to the film.

The IV measurements show asymmetric conduction through molecule **1**. Larger currents are seen under positive bias V than on negative V, provided $V \leq 1.5$ Volts, but if the scan range is extended to ± 2.0 Volts or above, then larger currents are seen at negative V. The "Janus-like" reversal of enhanced currents at higher biases reminds us of the two faces of Janus, the Roman god of war and peace. Even though several monolayer rectifiers could be studied in our laboratory well beyond ±1.0 Volts without electrical breakdown[2], the Janus behavior documented here was previously observed only for one of them (**Fig. 16** structure **12**)[3].

There is scatter in the measured currents and rectification ratios: this is fairly typical for such monolayer measurements. That the currents at increasing bias are affected differently than the currents at decreasing bias may be due to capacitance effects. Skeptics may wonder about molecular integrity under such large electric fields, but the repeatability of the asymmetrical conduction over so many measurements proves that the molecules have not been destroyed.

Resonance with the donor and/or acceptor levels may be used to explain the enhanced currents seen at sufficiently large forward (RR) or reverse (RRR) bias: this interpretation may not be fool-proof, but does seem to be at least plausible. Using the graphically estimated onset and rectification voltages for enhanced currents in the forward (**Fig. 8**) and reverse (**Fig. 9**) directions and the HOMO and LUMO energies from **Table A**, **Fig. 17** provides rough estimates for the donor and affinity levels. The roughly estimated V_{onset1} = 0.4 Volts (**Fig. 8**) is reasonably close to the transition voltage $|V_{tr}|$ = 0.47 to 0.54 V (**Fig. 14**): thus V_{tr} is a significant datum[53,55,56] (Eq. (5) or Eq. (6)), provided that the scan range does not exceed ±1 Volts.

Fig. 18 summarizes our thinking about what happens at zero bias (**Fig. 18(b)**), at sufficiently positive bias $V_{rect1}>0$ (**Fig. 18(a)**), and at sufficiently negative bias $V_{rect2}<<0$ (**Fig. 18(c)**). The single-molecule ε_{HOMO} and ε_{LUMO} levels are referenced to the zero-bias case, **Fig. 18(b)**, but, as donor levels and affinity levels, respectively, they shift (open arrows) downwards in **(a)** and

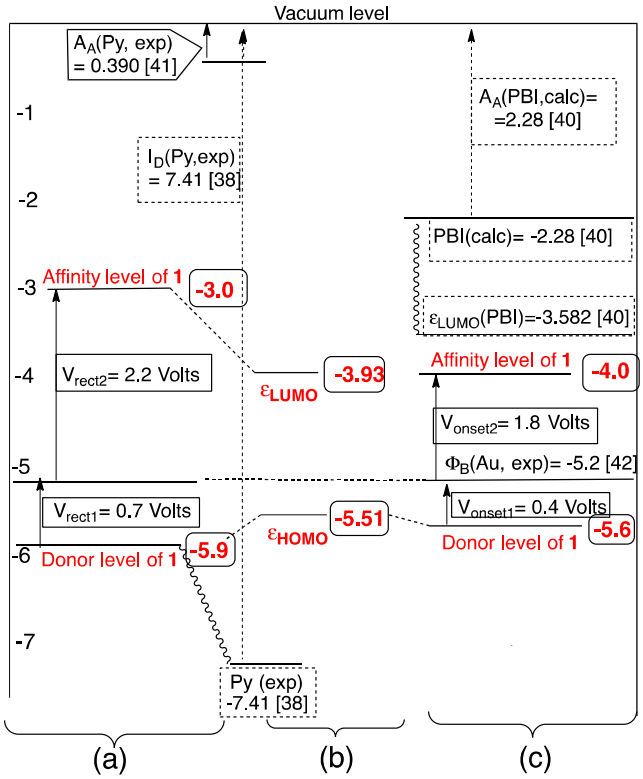

Fig. 17. Two estimates of the donor and affinity levels (eV, approximately to scale) for **1** in the sandwich "Au | monolayer of **1** | Au". The present results are boxed, the other values are from the [literature]: **(a)** Using onset voltages. **(b)** Isolated molecule. **(c)** Using rectification voltages.

upwards in **(c)**, until resonance is reached with the bias-shifted metal Fermi level.

In **Fig. 18(a)** resonant electron tunneling (1) from the donor level (shifted ε_{HOMO}) to right electrode is followed by tunneling (2) from left electrode to the shifted ε_{HOMO}. In **Fig. 18(c)** two different mechanisms, (A) and (B), are proposed for the reverse rectification. In mechanism (A), independent processes involve the donor level and the affinity level separately (numbered steps in round parentheses): (1) resonant tunneling from right electrode to the acceptor level (shifted ε_{LUMO}) followed by (2) tunneling to the left electrode; and (3) tunneling from the donor level (shifted ε_{HOMO}) to the left electrode, followed by (4) tunneling from the right electrode to ε_{HOMO}. In mechanism (B) [numbered steps in square brackets] there is [1] an "anti-Aviram-Ratner"[2] field-assisted pre-excitation from the shifted donor level to the shifted affinity level, [2] resonant tunneling from the acceptor level to the left electrode, and a second resonant tunnelling[7] from the right electrode to the shifted ε_{HOMO}; the direction of favored electron flow, from the Au pad to the bottom Au electrode is shown as an open arrow at the bottom.

The results reported here cannot discriminate between mechanisms (A) and (B) of **Fig. 18(c)**, but clearly are inconsistent with the original Aviram-Ratner formulation[1], which would show a direction of favored electron flow between the Au electrodes as the opposite of what we observed.

We have demonstrated beyond any reasonable doubt that the IV experiments can be cycled very many times between forward and reverse rectification, depending on the maximum voltage chosen, and that the sandwiches are sturdy, especially after many months

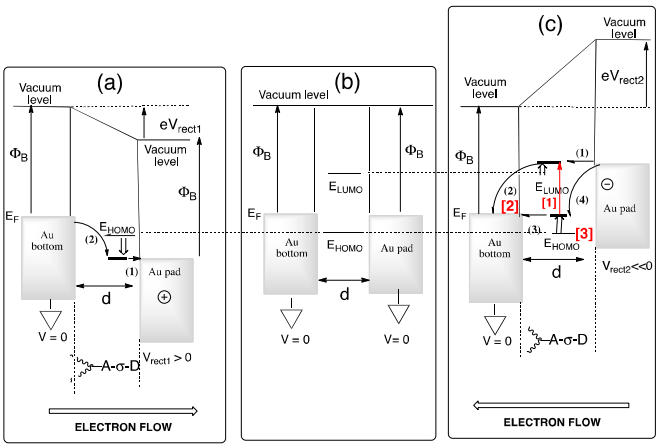

Fig. 18. (a) Rectification in the forward direction. (b) Zero-bias case, V = 0: no current flow. **(c) Rectification in the reverse direction.** For **(a)** and **(c)** the overall enhanced electron flow is shown as a closed double arrow.

and partial chemisorption.

What remains to be developed is a convenient semi-empirical "master equation" that could track these unusual electronic phenomena and provide estimates of transition energies between different transport mechanisms.

5. Conclusions

The donor-bridge-acceptor-tail molecule **1**, when placed as a Langmuir-Blodgett monolayer between Au electrodes, has been shown to be a direct-current rectifier in the forward direction if the bias range is limited to ≤1.5 Volts, but in the reverse direction at biases between -1.5 to -2.5 Volts. The *IV* data and their interpretation have been buttressed by theory, XPS, ellipsometry, and electrochemistry.

Dispassionate observers keep asking whether unimolecular electronics[2] will ever be technologically useful. The field is still at the component stage, with the construction of single-molecule rectifiers (and therefore also capacitors) and resistors (molecular wires). Missing is a unimolecular amplifier with power gain (we have proposed one[64]). The reliability of electrical measurements of single molecules and of monolayers has improved greatly (we provide here ample proof of the reliability of one rectifier). Integrating these single-molecule components into nano-circuits remains an on-going challenge.

6. Acknowledgments

This research was supported by the United States National Science Foundation (CHE-08-48206). One of us (MSJ) is grateful to Mr. Robert Holler for training on the XPS spectrometer, to Prof. Gregory J. Szulczewski for help in interpreting the XPS spectra, to Prof. Gary Mankey for training on the spectroscopic ellipsometer, and to the University of Alabama Machine Shop for assisting in all these experiments. DAD and MV were supported by the Chemical Sciences, Geosciences and Biosciences Division, Office of Basic Energy Sciences, U.S. Department of Energy (DOE) under grant no. DE-FG02-03ER15481 (catalysis center program) and by the Robert Ramsay Endowment of The University of Alabama.

7. Notes and References

[a] Laboratory for Molecular Electronics, Chemistry Department, University of Alabama, Tuscaloosa, AL 35487-0336, USA
[b] School of Pharmacy, University of Southern California, Los Angeles, CA 90089, USA
[c] Chemistry and Biochemistry Department, University of Mississippi, University, MS 38677, USA
[d] Chemistry Department, University of Alabama, Tuscaloosa, AL 35487-0336, USA

Electronic Supplementary Information (**ESI**) available: [Orbital energies; electrochemical potential spectrum; *I*-*A* isotherms and their change over time; polarized visible-UV spectra; AFM image; *IV* asymmetry for EGaIn; summary of *IV* data; full *IV* data; for each pad, curves for *I* vs. *V*, $\ln_e|I|$ vs. *V* and $\ln_e$ ($|I|V^{-2}$); trends for repeated *IV* runs]. See DOI: 10.1039/b000000x/

1 A. Aviram and M. A. Ratner, *Chem. Phys. Lett.,* 1974, **29**: 277.
2 R. M. Metzger and D. L. Mattern, *Top. Curr. Chem.,* 2012, **313**: 39.
3 A. Honciuc, R. M. Metzger, A. Gong, and C W. Spangler, *J. Am. Chem. Soc*., 2007, **129:** 8310.
4 I. Díez-Pérez, J. Hihath, Y. Lee, L. Yu, L. Adamska, M. Kozhushner, I. I. Oleynik, and N. Tao, *Nature Chem*., 2009, **1**: 635.
5 L. Jiang, L. Yuan, L. Cao, and C. A. Nijhuis, *J. Am. Chem. Soc.,* 2014, **136**: 1982.
6 I. Bâldea, *Phys. Rev. B*, 2012, **85***:* #035442.
7 W. J. Shumate, D. L. Mattern, A. Jaiswal, J. Burgess, D. A. Dixon, T. R. White, A. Honciuc, and R. M. Metzger, *J. Phys. Chem. B,* 2006, **110***:* 11146.
8 R. Kota, R. Samudrala, and D. L. Mattern, *J. Org. Chem*., 2012, **77**: 9641.
9 R. M. Metzger, T. Xu, and I. R. Peterson, *J. Phys. Chem. B,* 2001, **105**: 7280.
10 M. L. Chabinyc, X. Chen, R. E. Holmlin, H. Jacobs, H. Skulason, C. D. Frisbie, V. Mujica, M. A. Ratner, M. A. Rampi, and G. M. Whitesides, *J. Am. Chem. Soc.,* 2002, **124**: 11731.
11 R. C. Chiechi, E. A. Weiss, M. D. Dickey, and G. M. Whitesides, *Angew. Chem. Int. Ed*., 2008, **47**: 142.
12 M. D. Dickey, R. C. Chiechi, R. J. Larsen, E. A. Weiss, D. A. Weitz, and G. M. Whitesides, *Adv. Funct. Mater.,* 2008, **18**: 1097.
13 C. Nijhuis, W. F. Reus, and G. M. Whitesides, *J. Am. Chem. Soc*., 2009, **131**: 17814.
14 L. D. Landau and E. M. Lifschitz, *Quantum Mechanics Non-Relativistic Theory*, (translated by J. B. Sykes, and J. S. Bell) (Pergamon Press Ltd., London, 1958).
15 R. H. Fowler and L. Nordheim, *Proc. Roy. Soc. London,* 1928, **119**: 173.
16 J. G. Simmons, *J. Appl. Phys.,* 1963, **34**: 2581.
17 J. G. Simmons, *J. Appl. Phys*., 1963, **34**: 1793.
18 J. G. Simmons, *J. Phys. D,* 1971, **4**: 613-657.
19 R. Stratton, *J. Phys. Chem. Solids,* 1962, **23**: 1177.
20 D. M. Newns, *Phys. Rev*. 1969, **178**: 1123.
21 P. W. Anderson, *Phys. Rev*. 1961, **124**: 41.
22 V. Mujica, M. Kemp, A. Roitberg, and M. Ratner, *J. Chem. Phys*., 1996, **104**: 7296.
23 I. R. Peterson, D. Vuillaume, and R. M. Metzger, *J. Phys. Chem.,* 2001, **A105**: 4702.
24 L. E. Hall, J. R. Reimers, N. S. Hush, and K. Silverbrook, *J. Chem. Phys.,* 2000, **112**: 1510.
25 W. Wang, T. Lee, and M. A. Reed, *Phys. Rev. B* 2003, ***68***: #035416.
26 J. J. P. Stewart. *J. Molec. Model.*, 2007, **13**: 1173.
27 R. Bauernschmitt, R. Ahlrichs, *Chem. Phys. Lett.* 1996, **256**: 454.

28 M. E. Casida, C. Jamorski, K. C. Casida, D. R. Salahub, *J. Chem. Phys.* 1998, **108**: 4439.
29 A. D. Becke, *J. Chem. Phys.*, 1993, **98**: 5648.
30 C. Lee, W. Yang, R. G. Parr, *Phys. Rev. B,* 1988, **37**: 785.
31 N. Godbout, D. R. Salahub, J. Andzelm, E. Wimmer, *Can. J. Chem.* 1992, **70**: 560.
32 J. Tomasi, B. Mennucci, R. Cammi, *Chem. Rev.* 2005, **105**: 2999.
33 A. Klamt, G. Schüürmann, *J. Chem. Soc. Perkin Trans.* 1993, **2**: 799.
34 A. Klamt, *COSMO-RS: from quantum chemistry to fluid phase thermodynamics and drug design, Volume 1*; (Elsevier, Amsterdam, 2005).
35 Gaussian 09, Revision D.01, M. J. Frisch, G. W. Trucks, H. B. Schlegel, G. E. Scuseria, M. A. Robb, J. R. Cheeseman, G. Scalmani, V. Barone, B. Mennucci, G. A. Petersson, H. Nakatsuji, M. Caricato, X. Li, H. P. Hratchian, A. F. Izmaylov, J. Bloino, G. Zheng, J. L. Sonnenberg, M. Hada, M. Ehara, K. Toyota, R. Fukuda, J. Hasegawa, M. Ishida, T. Nakajima, Y. Honda, O. Kitao, H. Nakai, T. Vreven, J. A. Montgomery, Jr., J. E. Peralta, F. Ogliaro, M. Bearpark, J. J. Heyd, E. Brothers, K. N. Kudin, V. N. Staroverov, R. Kobayashi, J. Normand, K. Raghavachari, A. Rendell, J. C. Burant, S. S. Iyengar, J. Tomasi, M. Cossi, N. Rega, J. M. Millam, M. Klene, J. E. Knox, J. B. Cross, V. Bakken, C. Adamo, J. Jaramillo, R. Gomperts, R. E. Stratmann, O. Yazyev, A. J. Austin, R. Cammi, C. Pomelli, J. W. Ochterski, R. L. Martin, K. Morokuma, V. G. Zakrzewski, G. A. Voth, P. Salvador, J. J. Dannenberg, S. Dapprich, A. D. Daniels, Ö. Farkas, J. B. Foresman, J. V. Ortiz, J. Cioslowski, and D. J. Fox (Gaussian, Inc., Wallingford CT, 2009).
36 H. Eckhard, L. W. Shacklette, K. Y. Jen, and R. L. Elsenbaumer, *J. Chem. Phys.*, 1989, **91**: 1303.
37 R. Hesse, P. Streubel, and R. Szargan, *Surf. Interface Anal*., 2007, **39**: 381.
38 E. Clar, J. M. Robertson, R. Schloegl, and W. Schmidt, *J. Am. Chem. Soc*., 1981, **103**: 1320.
39 C.-G. Zhan, J. A. Nichols, and D. A. Dixon, *J. Phys. Chem. A*, 2003, **107**: 4184.
40 M. C. Ruiz Delgado, E.-G. Kim, D. A. da Silva Filho, and J.-L. Brédas, *J. Am. Chem. Soc*., 2010, **113:** 3375.
41 W. E. Wentworth and R. S. Becker, *J. Am. Chem. Soc.,* 1962, **84***:* 4263.
42 G. V. Hansson and S. A. Flodstrom, *Phys. Rev. B*, 1978, **18**: 1572.
43 S**.** Hirata, C.-G. Zhan, E. Apra, T. L. Windus, and D.A. Dixon, *J. Phys. Chem. A.,* 2003, **107**: 10154.
44 M. E. Peover and B. S. White, *Electroanal. Chem. Interf. Chem*., 1967, **13**: 93-99.
45 B. Wang, Z. Zhao, C. Cui, M. Wang, Z Wang, and Q. He, *Optical Mater*., 2012, **34***:* 1095.
46 J. Saalbeck, H. Kunkely, H. Langhals, R. W. Saalfrank, and J. Daub, *Chimia,* 1989, **43**: 6.
47 Z. Chen, V. Stepanenko, V. Dehm, P. Prins, L. D. A. Siebbeles, J. Seibt, P. Marquetand, V. Engel, and F. Würthner, *Chem. Eur. J.,* 2007, **13**: 436.
48 P. Wang, M. Shamsuzzoha, X.-L. Wu, W.-J. Lee, and R. M. Metzger, *J. Phys. Chem.,* 1992, **96**: 9025.
49 B. de Boer, A. Hadipour, M. M. Mandoc, T. van Woudenbergh, and P. W. M. Blom, *Adv. Mater*., 2005, **17**: 621.
50 Z. Huang. B. Xu, Y. Chen, M. Di Ventra, and N. Tao, *Nano Lett.,* 2006, **6**: 1240.
51 A. Jaiswal, D. Rajagopal, M. V. Lakshmikantham, M. P. Cava, and R. M. Metzger, *Phys. Chem. Chem. Phys.*, 2007, **9**: 4007.
52 J. M. Beebe, B. Kim, J. W. Gadzuk, C. D. Frisbie, and J. G. Kushmerick, *Phys. Rev. Lett.*, 2006, **97**: #026801.
53 J. M. Beebe, B. Kim, C. D. Frisbie, and J. G. Kushmerick, *ACS Nano,* 2008, **2**: 827.
54 E. H. Huisman, C. M. Guédon, B. J. van Wees, and S. J. van der Molen, *Nano Lett.,* 2009, **11**: 3909.
55 I. Bâldea, *Chem. Phys*. 2012, **400**: 65.
56 H. Song, Y. Kim, Y. H. Jang, H. Jeong, M. A. Reed, and T. Lee, *Nature,* 2009, **462**: 1039.
57 A. Honciuc, A. Otsuka, Y.-H.Wang, S. K. McElwee, S. A. Woski, G. Saito, and R. M. Metzger, *J. Phys. Chem. B,* 2006, **110**: 15085.
58 A. Jaiswal, D. Rajagopal, M. V. Lakshmikantham, M. P. Cava, and R. M. Metzger, *Phys. Chem. Chem. Phys.* 2007, **9**: 4007.
59 J. W. Baldwin, R. R. Amaresh, I. R. Peterson, W. J. Shumate, M. P. Cava, M. A. Amiri, R. Hamilton, G. J. Ashwell, and R. M. Metzger, *J. Phys. Chem*. B 2002, **106**: 12158.
60 R. M. Metzger, J. W. Baldwin, W. J. Shumate, I. R. Peterson, P. Mani, G. J. Mankey, T. Morris, G. Szulczewski, S. Bosi, M. Prato, A. Comito, and Y. Rubin, *J. Phys. Chem. B,* 2003, **107**: 1021.
61 A. Honciuc, A. Jaiswal, A. Gong, K. Ashworth, C. W. Spangler, I. R. Peterson, L. R. Dalton, and R. M. Metzger, *J. Phys. Chem. B,* 2005, **109**: 857.
62 W. J. Shumate, D. L. Mattern, A. Jaiswal, J. Burgess, D. A. Dixon, T. R. White, A. Honciuc, and R. M. Metzger, *J. Phys. Chem. B*, 2006, **110**: 11146.
63 W. J. Shumate, Ph. D. dissertation (Univ. of Alabama, **2005)**.
64 C. Toher, D. Nozaki, G. Cuniberti, and R. M. Metzger, RSC Nanoscale 2013, **5**: 6975.

A new monolayer rectifier with pyrene donor (D) and perylenebisimide acceptor (A) rectifies A→D below 2.0 Volts, but A←D beyond that.